N72-23793

MIXING EFFECTIVENESS IN THE APOLLO OXYGEN TANKS OF SPIN-UP AND ROTATION-REVERSAL MANEUVERS

By Barrett Baldwin, E. Dale Martin, Walter A. Reinhardt, and Yvonne Sheaffer

Ames Research Center, NASA, Moffett Field, Calif. 94035

Abstract

Two-dimensional simulations of stratified flows in the Apollo oxygen tanks have been used to estimate the mixing effectiveness of spin-up and rotation-reversal maneuvers. Calculations have been made for square and circular cylindrical tank geometries. Differences arising from heater position on the tank wall or near the center of the tank have been investigated. In the event of a prolonged period without normal maneuvers, our investigations show that the potential pressure decay (drop in pressure that would result from adiabatic mixing) can be suppressed by more than a factor of two through the use of spin-up and rotation-reversal maneuvers. Changes in rotation rate of order three revolutions per hour or greater are sufficient for this purpose.

Introduction

Analyses of Apollo 12 data by several investigators (ref. 1) indicated that no serious stratification problems were to be expected from operation of the Apollo oxygen tanks with the mixing fans removed. This expectation was reinforced by the successful Apollo 14 flight during which additional information was secured. The view might be adopted that further investigation of a working system is not necessary. Yet in view of the serious consequences that could result from an undisclosed weakness it seems worthwhile to understand the operation of all parts of the system as thoroughly as possible.

Theoretical investigations of the degree of stratification to be expected in the absence of convection have indicated that potential pressure decays amounting to several hundred psi could develop (refs. 2 and 3). The pressure drops that would result from sudden mixing according to these predictions would not interfere with the operation directly. But a two-phase mixture could be produced in the oxygen tanks with possible damaging consequences elsewhere in the system. On the other hand, stratification analyses, which account for convection as well as conduction, indicate that excessive buildup of the potential pressure decay is averted by the mixing that results from normal vehicle maneuvering (refs. 4 and 5). Much as in the case of an earthquake, it is better to undergo numerous small maneuvers rather than a prolonged period of quiet followed by a big one.

Pressure and temperature data from past Apollo flights is useful for understanding the relationship between maneuvers and conditions in the oxygen tanks. However, direct measurements of velocity and temperature distributions in the tanks have not been made. At present the best information on detailed conditions in the tanks is based on two-dimensional computational simulations of the stratified flows resulting from maneuvers.

In this paper results are presented from a series of such calculations utilizing the methods described in references 5 through 10. Preliminary results based on the van der Waals equations of state were presented at meetings on the Apollo oxygen system held at the Manned

Spacecraft Center prior to the Apollo 14 flight. It was concluded by participants at the meetings that normal vehicle maneuvering could be relied upon to produce the necessary mixing. Nevertheless, several investigations were made of emergency procedures that could be used if the performance fell below the predicted level. Two-dimensional numerical simulations of stratified oxygen flows indicated that vehicle maneuvering leading to acceleration fields of order 10^{-3} g lasting for several seconds would produce effective mixing (ref. 4). The question was also raised whether reversal of the rotation rate starting at 3 revolutions/hour would provide useful mixing action in the oxygen tanks. From our preliminary results based on the van der Waals equations it was concluded that this latter maneuver would indeed provide an effective backup means for mixing the oxygen if normally occurring maneuvers proved insufficient. That conclusion is of continuing interest for future Apollo flights in which vehicle maneuvering is relied upon to produce the necessary mixing in the oxygen tanks.

In this paper we present results from calculations based on the accurate thermodynamic relations described in reference 8. The preliminary conclusions are verified and put on a firmer basis by these results. The effect of changes in rate of rotation on additional types of stratification are investigated. Preliminary calculations showing the rate of buildup of potential pressure decay during heater cycling are described.

Analytical Method

A two-dimensional square tank geometry similar to that of references 4 and 5 is utilized for the numerical simulation. The integration procedure used for the results in this paper is described in references 6 and 9. The equations expressing conservation of mass, momentum, and energy are cast in a form in which the primary dependent variables are the vorticity and temperature distributions. A pair of coupled differential equations results. A predictor-corrector method is used in the numerical differencing procedure. A time-dependent temperature distribution is determined from the integration. Several approximations are employed. Although pressure gradients must be considered in the momentum equations, it can be shown that for the low-velocity cryogenic oxygen flows under consideration, pressure gradients can be neglected in the energy equation. Likewise, the variations in pressure with time have only a cumulative effect in the energy equation that does not affect the motion of the gas directly. The most important coupling between the momentum and energy equations is through temperature gradients and convection of temperature variations. As a result, for the purpose of finding the motion of the gas, the density can be considered a function of temperature with pressure as a slowly varying parameter. If the temperature variations are sufficiently mild, the density and enthalpy can be approximated by the first several terms of series

expansions in temperature with coefficients that vary slowly in time due to cumulative changes in pressure and temperature level. The derivation in reference 6 shows that to lowest order the flow equations can be cast in a form that is then independent of pressure and density variations. The corresponding integration procedure described in reference 9 requires as input a mean density $\overline{\rho}$ and thermal expansion coefficient β, each of which can be time dependent to allow for cumulative changes in pressure and temperature level. A time-dependent temperature distribution results from the integration procedure. The purpose of this section is to indicate how such output can be interpreted to determine the attendant slowly varying pressure as well as other thermodynamic variables such as the density distribution and the potential pressure decay that would result from adiabatic mixing.

As far as the thermodynamic state of the gas is concerned, pressure gradients are negligible at the low velocities that occur in a cryogenic oxygen storage tank in a near-zero gravitational environment. The pressure can therefore be considered uniform in the tank. The kinetic energy associated with the motion of the gas is also negligible compared to changes in the internal energy of interest. Thus the problem to which we shall address ourselves here is that of evaluating the time-dependent thermodynamic state of a stationary stratified gas from a knowledge of the time-dependent mean density and temperature distribution. The degree of rigor brought to bear is independent of the means used to arrive at the input information on mean density and temperature distribution. The methods developed for this purpose would, therefore, be applicable to the results from more accurate three-dimensional analyses of the convection and conduction processes within the tank. We have considered the problem at two levels of rigor. In preliminary work (ref. 5), the van der Waals equations of state were employed and in this paper we include results based on the accurate thermodynamic relations developed in reference 8.

Approximate Procedure Based on van der Waals Equations

As discussed above, the problem at hand is to find the pressure and other thermodynamic quantities when the mean density and temperature variation in the tank are known. The mean density $\overline{\rho}$ is known in terms of the total mass of oxygen M from the relation

$$\overline{\rho} = M/V_T \tag{1}$$

where V_T is the tank volume. A method for including the effect of tank stretch on the rate of pressure rise, not included in this description, is given in reference 7. The rate of change of mean density is found by differentiation

$$\frac{d\overline{\rho}}{dt} = \frac{(dM/dt)}{V_T} \tag{2}$$

where dM/dt is the rate of gas removal (typically, 0 to 3 lbm/hr). Values of $\overline{\rho}$ are computed at each time step from the relation

$$\overline{\rho}_{t+\Delta t} = \overline{\rho}_t + \Delta t \frac{(dM/dt)}{V_T} \tag{3}$$

using input values of dM/dt and V_T which are held constant during the integration.

At each time step the values of temperature T_{jk} at the computational grid points are determined from the integration procedure. The corresponding densities ρ_{jk} are computed to lowest order from the relation

$$\rho = \overline{\rho}[1 - \beta(T - \overline{T})] \tag{4}$$

where $\overline{T}$ is the volume average of the temperature variation T_{jk} and $\beta = -(1/\rho)(\partial\rho/\partial T)_p$ is the coefficient of thermal expansion corresponding to the state $\overline{\rho}$, $\overline{T}$. The van der Waals equation for pressure p is

$$p = \frac{RT\rho}{1 - b\rho} - a\rho^2 \tag{5}$$

Differentiation leads to the relation

$$\beta = \frac{R(1 - b\rho)}{RT - 2a\rho(1 - b\rho)} \tag{6}$$

for the coefficient of thermal expansion. In our preliminary results a constant value of β evaluated at the initial values of $\overline{\rho}$ and $\overline{T}$ was used.

Since a uniform spacing of computational grid points is employed in the integration procedure, the volume average $\overline{T}$ can be computed according to the relation

$$\overline{T} = \frac{\sum_{j,k} T_{j,k} W_{j,k}}{\sum_{j,k} W_{j,k}} \tag{7}$$

where $W_{j,k}$ is a weighting function that is taken equal to 1.0 at interior points, 0.5 at boundary points except in the corners, and 0 in the corners. The corners are excluded (zero weight) because, in the integration procedure described in reference 9, temperatures at the corners are not used and are not computed.

Substitution of T_{jk} and ρ_{jk} into equation (5) would lead to pressures p_{jk} that are not all equal. Since the pressure should be uniform in the tank, it is expedient to evaluate an average pressure according to the relation

$$\overline{(p + a\rho^2)(1 - b\rho)} = R\overline{T\rho}$$

where the bar indicates a volume average of the same type as in equation (7). Substitution of equation (4) into this relation, use of the fact that $\overline{(T - \bar{T})} = 0$, and omission of $\overline{(T - \bar{T})^3}$ terms lead to the approximate expression

$$p = \frac{R\bar{T}\bar{\rho}}{1 - b\bar{\rho}} - a(\bar{\rho})^2 + \frac{[a(\bar{\rho})^2(3b\bar{\rho} - 1)\beta^2 - R\bar{\rho}\beta]\overline{(T - \bar{T})^2}}{1 - b\bar{\rho}} \tag{8}$$

for the pressure in terms of average density, average temperature, and mean squared deviation of the temperature from the average value. The latter quantity is computed at each time step as in equation (7) according to the relation

$$\overline{(T - \bar{T})^2} = \frac{\sum_{j,k} (T_{jk} - \bar{T})^2 W_{jk}}{\sum_{j,k} W_{jk}} \tag{9}$$

In addition to the pressure, the potential pressure decay that would result from complete adiabatic mixing is of interest. In general, the procedure for evaluation of this quantity is as follows:

$M = \overline{\rho}V_T$	total mass
$E = \overline{e\rho}V_T$	total internal energy
$e_c = E/M$	specific internal energy of collapsed state resulting from complete adiabatic mixing
$\rho_c = \rho/(1 - K_S)$	density of collapsed state
$T_c = T(e_c, \rho_c)$	temperature of collapsed state
$p_c = p(T_c, \rho_c)$	collapse pressure
$p - p_c$	potential pressure decay

where e is the specific internal energy and $\overline{e\rho}$ is a volume average. The factor $(1 - K_S)$ allows for shrinkage of the tank volume due to a drop in pressure and can be evaluated from the relation (ref. 4)

$$K_S = \frac{3r(1 - \sigma)(p - p_c)}{2b_1 E_y}$$

where

r/b_1 = ratio of spherical tank radius to wall thickness

σ = Poisson's ratio for tank wall material

E_y = Young's modulus for tank wall material

Evaluation of the tank stretch effect requires iterative solution for K_S and $p - p_c$. Recently, we have made calculations in which this procedure is included.

The above procedure for determination of the potential pressure decay can be carried out using approximate equations of state or the more exact relations of reference 8. Our preliminary results were based on the van der Waals equations of state, equation (5), and (ref. 11)

$$e = c_1 + c_v T - a\rho \tag{10}$$

Substitution of equation (5) into (10) to eliminate the temperature and use of the fact that the pressure is uniform in the initial stratified state yield the formula

$$p - p_c = \frac{ab[\overline{\rho^3} - (\overline{\rho})^3] - a[1 - (R/c_v)][\overline{\rho^2} - (\overline{\rho})^2]}{1 - b\overline{\rho}}$$

where $\overline{\rho^2}$ and $\overline{\rho^3}$ indicate volume averages. Substitution of the first-order density relation, equation (4), rearrangement, and omission of $\overline{(T - \overline{T})^3}$ terms lead to the approximation

$$p - p_c = \frac{a(\overline{\rho})^2[3b\overline{\rho} - 1 + (R/c_v)]\beta^2\overline{(T - \overline{T})^2}}{1 - b\overline{\rho}} \tag{11}$$

which expresses the potential pressure decay in terms of the average density and mean squared deviation of temperature from the average value.

The specific heat at constant pressure is needed in the integration procedure described in references 6 and 9. The van der Waals equations of state (eqs. (5) and (10)) can be used to derive the relation

$$c_p = c_v + \frac{R}{1 - 2a\rho(1 - b\rho)^2/RT} \tag{12}$$

In our preliminary results a constant value of c_p was used, evaluated at the initial values of $\overline{\rho}$ and $\overline{T}$. The values of the constants R, b, a, c_v used in the van der Waals equations were chosen such that the critical pressure, temperature, and density are matched exactly according to relations given by Hirschfelder, Curtiss, and Bird (ref. 11).

Procedure Based on Exact Thermodynamics

In this section an exact method is described for finding the pressure and other thermodynamic quantities when the mean density and temperature distribution in the tank are known. For this purpose it was found expedient to determine a temperature distribution function $F_T(N)$ of the type developed in reference 8 rather than to consider thermodynamic quantities at each computational grid point. The function $F_T(N)$ is defined to be a weighted number of computational grid points with temperatures between $T_N - \Delta T$ and $T_N + \Delta T$ where the T_N are a fixed array of temperatures with uniform spacing equal to ΔT. The weighting employed is proportional to the volume associated with each computational grid point. Interior points are given a weight $w_{jk} = 1.0$, for boundary points $w_{jk} = 0.5$ and the corner points are given zero weight since their temperatures are not computed in the integration procedure. For each value of j and k, w_{jk} is assigned to the two $F_T(N)$ between which its temperature lies in proportion to its proximity to each; that is, if $T_N < T_{jk} < T_{N+1}$, $F_T(N)$ is increased by an amount $w_{jk}(T_{N+1} - T_{jk})/\Delta T$ and $F_T(N+1)$ is increased by an amount $w_{jk}(T_{jk} - T_N)/\Delta T$. Thus the sum

$$\sum_{N=1}^{N_{MAX}} F_T(N)$$

is equal to the total number of interior computational grid points plus half the number of boundary points, not counting corners. The quantity $F_T(N)$ is essentially equal to the total number of computational grid points with temperature between $T_N - (1/2)\Delta T$ and $T_N + (1/2)\Delta T$ except for a small readjustment corresponding to a linear interpolation. Figure 1 shows an example of a temperature distribution $F_T(N)$ plotted

versus T_N. Additional examples and further discussion of the meaning of this distribution function are contained in references 7, 8, and 10.

An array of temperatures T_N is associated with the temperature distribution function $F_T(N)$. At a given tank pressure p, associated arrays of density ρ_N and internal energy e_N can be computed according to the relations

$$\rho_N = \rho(p, T_N) \tag{13}$$

$$e_N = e(\rho_N, T_N) \tag{14}$$

The computation of the functions $\rho(p, T_N)$ and $e(\rho_N, T_N)$ is described in reference 8. Since the $F_T(N)$ are proportional to the volume of gas in the temperature range $T_N - (1/2)\Delta T$ to $T_N + (1/2)\Delta T$, the volume averages $\overline{\rho}$ and $\overline{\rho e}$ can be computed according to

$$\overline{\rho} = \frac{\sum_{N=1}^{N_{MAX}} F_T(N)\rho_N}{\sum_{N=1}^{N_{MAX}} F_T(N)} \tag{15}$$

$$\overline{\rho e} = \frac{\sum_{N=1}^{N_{MAX}} F_T(N)\rho_N e_N}{\sum_{N=1}^{N_{MAX}} F_T(N)} \tag{16}$$

Values of gas density and the transport properties at the computational grid points are found by linear interpolation of values computed at the conditions ρ_N, T_N.

At the beginning of an integration for the time-dependent temperature distribution, a tank pressure p and values of temperature T_{jk} at the computational grid points are specified. The distribution function $F_T(N)$ is computed and the above relations are used to determine the initial values of $\overline{\rho}$ and $\overline{\rho e}$. In the subsequent integration the variation of $\overline{\rho}$ is computed from equations (3) and depends on the specified constant rate of gas removal dM/dt. The values of T_{jk} resulting from the integration are used to compute $F_T(N)$ at the end of each time step. The problem then arises of computing the change in pressure p

in each time step. By differentiation it can be seen that changes in the ρ_N are related to changes in pressure according to

$$\Delta\rho_N = \frac{\Delta p}{(\partial p/\partial \rho_N)_{T_N}} \tag{17}$$

since the values of T_N are held fixed throughout the integration. Substitution of this in the relation

$$(\rho_N)_{n+1} = (\rho_N)_n + \Delta\rho_N \tag{18}$$

yields

$$(\rho_N)_{n+1} = (\rho_N)_n + \frac{\Delta p}{(\partial p/\partial \rho_N)_{T_N}} \tag{19}$$

where the subscript n refers to the time step in the integration. Multiplication of the last equation by $F_T(N)_{n+1}$, summation over N, and substitution of

$$\sum_{N=1}^{N_{MAX}} F_T(N)_{n+1}(\rho_N)_{n+1} = \overline{\rho}_{n+1} \sum_{N=1}^{N_{MAX}} F_T(N)_{n+1} \tag{20}$$

yield

$$\overline{\rho}_{n+1} \sum_{N=1}^{N_{MAX}} F_T(N)_{n+1} = \sum_{N=1}^{N_{MAX}} F_T(N)_{n+1}(\rho_N)_n + \Delta p \sum_{N=1}^{N_{MAX}} \frac{F_T(N)_{n+1}}{(\partial p/\partial \rho_N)_{T_N}} \tag{21}$$

Since $\overline{\rho}_{n+1}$ and $F_T(N)_{n+1}$ are known at the end of the (n+1)st time step, this equation can be used to compute the change in pressure Δp associated with the time step. Once Δp is known, equation (19) can be used to compute the updated values of density $(\rho_N)_{n+1}$. As a check, $\overline{\rho}_{n+1}$ can be computed using equation (20) for comparison with the imposed value of $\overline{\rho}_{n+1}$ from equation (3). Finally, the updated pressure is computed according to

$$p_{n+1} = p_n + \Delta p \tag{22}$$

The structure of equation (21) is such that the value of $\overline{\rho}_{n+1}$ computed from equation (20) will always be driven toward the imposed

value from equation (3) so that cumulative drifts cannot occur. Cumulative drifts of the individual $(\rho_N)_{n+1}$ computed from equation (19) can take place, however. To avoid this, at every tenth time step, the ρ_N are recomputed according to equation (13). It has been found that the foregoing procedure is quite stable and, for the sizes of time step imposed by stability criteria of the integration procedure, is quite accurate with a 1° K spacing of the temperature elements T_N. It can be noted that the foregoing procedure could not be applied at the computational grid points since equation (19) is valid only for an array of constant temperatures T_N.

Once the pressure is determined the potential pressure decay can be computed by the procedure described in reference 8 that utilizes the distribution function $F_T(N)$. As a check, the potential pressure decay can also be computed by the alternative method of reference 8 for which the pressure p and temperatures at computational grid points are utilized. Figure 2 shows a comparison of potential pressure decays computed by the two methods for a linear temperature distribution. The dashed lines indicate the potential pressure decay for each case computed exactly by evaluation of the thermodynamic quantities at all computational grid points. The symbols indicate values of the potential pressure decay computed using the distribution function $F_T(N)$ for various values of the temperature array spacing ΔT. It can be seen from the results in figure 2 that the temperature array spacing $\Delta T = 1°$ K provides adequate accuracy for all of the cases considered.

Method for Simulating Heater

An internal heater is used in the Apollo oxygen tanks to increase the pressure when it falls below 870 psia due to gas removal. In reference 4 a segment of the wall is used to simulate such a heater. It was found that the boundary-layer flow in the neighborhood of the heater cannot be adequately resolved with a uniform grid spacing when the acceleration field is of order 10^{-6} g or greater. Methods can nevertheless be found that lead to physically reasonable and qualitatively correct results if attention is confined to energy conservation, and accurate values of heater temperature are not required.

The energy balance will be properly maintained if at the beginning of each time step the heater element temperatures are increased by an amount ΔT_H corresponding to a specified heater power dQ/dt added to the total gas volume V_{HT} associated with the heater element computational grid points; that is,

$$\Delta T_H = \frac{(dQ/dt)\,\Delta t}{\rho C_p V_{HT}} \qquad \text{(before integration step)} \qquad (23)$$

The gas volume associated with each interior computational grid point is

$$V_H = \frac{V_T \, \Delta x \, \Delta y}{\ell_x \ell_y} \tag{24}$$

where Δx and Δy are the distances between grid points and ℓ_x, ℓ_y, the tank dimensions.

If the heater element computational grid points are interior points, the total heater gas volume V_{HT} is the number of heater elements times V_H. But heater volume elements on the boundary are half the value given in equation (24) since the boundary passes through the grid points. When the heater elements are in the interior their temperatures will rise until a balance is reached between the temperature increase from equation (23) and the decrease due to convection and conduction computed in the integration procedure. When the heater elements are on the boundary, however, the integration procedure does not modify their values. In that case, it is necessary to allow for a decrease in temperature at the *end* of each time step according to the amount of heat transferred to the interior grid points from the heater elements. The appropriate change in wall heater element temperatures is

$$\Delta T_H = - \frac{2K(T_H - T_{interior}) \, \Delta t}{C_p \rho (\Delta x)^2} \qquad \text{(after integration step)} \tag{25}$$

If the heater is on a wall, the ΔT_H computed in equation (25) corresponds to an insulated wall boundary condition except for a small (physically correct) lag due to the heat capacity of the gas adjacent to the wall.

The same type of computation as that in equations (23) and (25) can be used at all boundary points to simulate the heat leak from the exterior of the tank. In that case dQ/dt in equation (23) is replaced by the heat leak power dQ_L/dt.

The power radiated from the heater can be allowed for by means of the relation

$$\frac{dQ}{dt} = \frac{d\tilde{Q}}{dt} - Q_{RAD} \tag{26}$$

where $d\tilde{Q}/dt$ is the specified input heater power and

$$Q_{RAD} = \varepsilon \sigma_R [T_H^4 - (\overline{T})^4] A_H \tag{27}$$

where ϵ is the emissivity (typically, 0.32), σ_R the Stefan-Boltzmann constant, and A_H the heater area. According to reference 12, less than 10 percent of the radiated power is absorbed in the oxygen (usually much less depending on the heater temperature). Therefore, most of the radiation is absorbed in the tank wall and Q_{RAD} should be added to the heat leak power dQ_L/dt. In reference 7, methods for including the effects of tank stretch are described.

Results

Mixing Effectiveness of Rotation Reversal

Calculations were made in which the vehicle was taken to be rotating initially at 3 revolutions/hour. A series of initial stratified states were imposed with the temperature varying linearly across the tank. The hot gas was placed in the stable position toward the center of rotation outside the tank. Such stratification can be expected to develop after many heater cycles while operating with a steady vehicle rotation rate, although no heater was actually used in this first type of calculation. In the absence of other vehicle maneuvering and with the heater turned off, the calculations show a very slow decrease in potential pressure decay and no motion of the gas. The decrease in potential pressure decay in this case is due to conduction arising from the mild temperature gradient. When the direction of rotation is abruptly reversed, however, a swirling motion of the gas ensues and leads to mixing and enhanced temperature gradients. Figure 3 depicts the velocity field in the flow that results. Photographs are shown of a cathode ray display tube on which were plotted the velocity vectors at the computational grid points. The upper left photograph shows the velocities immediately after rotation reversal. The magnitude of the velocity near the tank boundaries is about 0.02 ft sec^{-1}. The clockwise swirling motion results in part from the rotational inertia of the gas which tends to retain the motion it possessed before the rotation reversal of the vehicle. A lateral linear acceleration, present during the reversal, acts differentially on the stratified layers to give an additional kick to the swirling motion. The other photographs in figure 3 show the velocity vectors at later times. The off-center swirl that develops because of the stratification present moves continuously in the clockwise direction which is also the direction of motion of the gas. The center of rotation is about 1-1/2 tank diameters below the center of the tank.

In addition to velocity vectors, several other features are visible in the photographs in figure 3. The arrow midway up on the right indicates the direction of the sun. The graph at the bottom is a running plot of the potential pressure decay versus time. The scale is automatically decreased when the plot becomes overextended. In the lower

right photograph the time scale has been decreased by a factor of 2 relative to that in the other photographs. The numerical values visible on the right represent the following quantities:

OMEG	vehicle rotation rate, radian sec^{-1}
DQDT	heater power, W
RHOB	mean density, g cm^{-3}
TB	mean temperature, °K
TH	heater temperature, °K
P	pressure, psia
DPC	potential pressure decay (method 1, ref. 8), psi
PPD	potential pressure decay (method 2, ref. 8), psi
COUNT	number of time steps in the integration

Method 1 of reference 8 utilizes a temperature distribution function, while method 2 uses temperatures at the computational grid points.

Figure 4 contains photographs showing the evolution of temperature distribution in the tank. For temperatures greater than the average, the deviations from the mean temperature are represented by vertical lines. As an aid to visualization, for temperatures less than average the deviations from the mean are shown as horizontal lines. In either case, the length of the lines indicates the magnitude of the temperature deviation from the mean at each computational grid point. The upper left photograph in figure 4 shows the initial assumed linear temperature distribution. The hot gas is toward the center of rotation, which is 1-1/2 tank diameters below the center of the tank. The remaining photographs show temperature distributions at later times after mixing has resulted from the swirling motion.

Figure 5 contains plots of the thermodynamic state of the gas without regard to position in the tank (see ref. 8). This is the number of computational grid points within 1° K temperature intervals. The unfilled histogram represents the initial linear temperature distribution. The shaded histogram shows the distribution 40 minutes after rotation reversal when considerable mixing has taken place and the steep temperature gradients have reduced the temperature deviations from the average temperature.

The variation of potential pressure decay with time for two cases is shown in figure 6. The curve labeled Stewart was computed using the accurate thermodynamic functions described in reference 8. The curve labeled van der Waals is from our preliminary report (ref. 5). The preliminary results compare favorably with those from the present more accurate calculations. In these runs no provision was made for heater cycling and the pressure dropped to about 700 psia as a result of the mixing. The mean density was held fixed corresponding to a zero rate of gas removal. The mean temperature remained constant at about 150° K.

The close agreement between the preliminary results based on the van der Waals equations and the present calculations is somewhat fortuitous. Figure 7 contains plots of potential pressure decay versus the magnitude of linear temperature variations for several tank pressures according to the van der Waals equations. Figure 8 shows results for the same conditions based on the accurate thermodynamics of reference 8. It is not necessary to superimpose figures 7 and 8 to see that the van der Waals results disagree grossly with those based on Stewart's equations when the pressure is held constant. However, for the rotation-reversal computations in which the pressure was allowed to decrease, the results in figure 6 show much smaller differences than would be expected from comparison of figures 7 and 8. The preliminary conclusions on the mixing effectiveness of the rotation-reversal maneuver, although not changed, have been put on a firmer basis by the calculations utilizing accurate thermodynamics in this paper.

The sharp bends in the curves contained in figure 8 are of interest. The flattening out takes place when a level of stratification is reached for which the collapsed state contains a two-phase mixture of liquid and vapor. Many other interesting aspects of the behavior of cryogenic oxygen are illustrated in the thermodynamic property plots presented in reference 8.

Figure 9 contains results based on accurate thermodynamics for several cases with less severe initial stratification. Decreases in potential pressure decay by a factor of 2 or more result from rotation reversal in these cases also. Most of the calculations in this paper were made with a value of 0.8 for the Courant number as defined in reference 9. Case I in figure 9 was also computed with a Courant number of 0.4. It can be seen that there is little difference. Appreciable variations in the flow variables extend over several computational grid points except in the boundary layer at the wall. Changes taking place in the boundary layer do not significantly affect the evolution of the potential pressure decay in the rotation-reversal problem. For this reason, as discussed in reference 5, the results are insensitive to a change in grid spacing from a 17 × 17 matrix to a 33 × 33 matrix.

Mixing Effectiveness of Spin-Up After Attitude Hold

In the previous section, initial stratified states were considered that would be expected to result after many heater cycles with the vehicle in the PTC mode (rotation at a steady rate). Another case of interest is the type of stratification that would result after many heater cycles in the attitude hold mode. In the absence of vehicle maneuvering no convection currents would develop and the heat from the heater can spread into the gas only by conduction. A localized hot spot around the heater somewhat diffused by conduction is to be expected in this case with essentially zero gas velocity. It is of interest to determine the mixing effectiveness on such an initial stratified state of a vehicle spin-up to the PTC mode. In the coordinate system fixed with respect to the tank used in this paper changes in rotation rate cause a rotating motion of the gas. The velocity field that occurs as a result of spin-up is similar to that shown in figure 3. Figure 10 illustrates the effect of spin-up on the temperature distribution. The upper left photograph shows the initial assumed distribution. Subsequent distortions and dissipation resulting from the swirling motion are shown in the remaining photographs.

Figure 11 is a plot of potential pressure decay versus time after spin-up. For comparison, a plot is included showing the very slow decrease in potential pressure decay that occurs as a result of conduction when the attitude hold condition is maintained. Again it is found that a change in vehicle rotation rate provides effective mixing action.

Flows and Stratified States Produced by Heater Cycles

Figure 12 shows the velocity fields that develop after several heater cycles for different tank geometries and heater positions. The flow field in the photograph on the upper left was generated with elements on the left wall acting as a heater. The plot at the bottom of the upper left frame is the potential pressure decay versus time from the beginning of the calculation. The potential pressure decay rises when the heater is on and subsides when the heater is off. It can be seen that about 6-1/2 heater cycles have taken place since the beginning of the calculation at the time of the photograph. A vehicle rotation rate of 0.4 revolution/hour was imposed in all of the cases shown in figure 12 corresponding to about 5×10^{-8} g at the center of the tank. Additional information on these runs is presented in subsequent figures. The meanings of the numerical values on the right of each frame was explained earlier in this paper in connection with figure 3.

In the upper right photograph of figure 12 the velocity field is shown for a calculation in which the heater is located near the center of the tank. The lower left frame contains similar results for a

circular cylindrical tank geometry with an off-center internal heater position. The lower right frame shows the temperature distribution in the tank corresponding to the same calculation. For times of order 2 hours with small vehicle rotation rates, only a small volume of gas near the heater is heated appreciably.

Figure 13 shows the pressure cycles and potential pressure decay versus time corresponding to the upper left frame of figure 12. The next two figures contain similar results corresponding to the other frames of figure 12. Comparison of these results indicates that the heater cycle durations and magnitudes of potential pressure decay are insensitive to the tank geometry and heater positions used in the calculations. However, the results do depend on the total volume associated with the computational grid points assigned as heater elements. The results in figures 13 to 15 correspond to a heater area of approximately 0.5 ft^2.

Figure 16 shows the effect of vehicle spin-up on the pressure cycle and the potential pressure decay. In this calculation a circular cylindrical tank geometry with off-center internal heater was employed. A smaller heater volume was used corresponding to a heater area of about 0.3 ft^2. During the initial buildup of potential pressure decay, the vehicle was not rotating. The spin-up was started at 127 minutes after the start of the calculation and was completed in about 5 minutes. The rotation rate was held constant at 3 revolutions/hour thereafter. After a delay of about 10 minutes the swirling motion of the gas introduced by the vehicle spin-up had a large effect on the pressure cycle. The potential pressure decay dropped off precipitously, causing a drop in pressure as well. Thus, even though the heater was turned on at 149 minutes when the pressure fell below 870 psia, the pressure continued to drop and was down to 810 psia at the end of the calculation. Thus the same conclusion on the mixing effectiveness of a change in vehicle rotation rate has been arrived at from a calculation in which the stratification was produced by heater cycling. Additional calculations have been made for tank quantities between 65 and 90 percent with similar results.

Conclusions

The foregoing results show that appreciable mixing can be achieved in a short time by changing the vehicle rotation rate by modest amounts. No significant differences were found in the calculations for square or circular cylindrical tank geometries. Results from calculations in which the heater was located on the wall did not differ grossly from those in which the heater position was near the center of the tank. Earlier predictions based on the van der Waals equations of state have been verified by the use of accurate thermodynamic relations.

It appears that changes in the vehicle rate of rotation by several revolutions per hour or greater could be used in the same way that the mixing fans were used in earlier Apollo flights for which fans were installed in the oxygen tanks. Namely, such a maneuver could be initiated if there is reason to believe that the level of stratification is high. Time lags of order 20 minutes to an hour are to be expected before effective mixing will occur after the maneuver is initiated. A spin-up followed by a spin-down in less than 20 minutes would be less effective than if the new rotational state were maintained for a longer period.

References

1. Anon.: Minutes of the Third Apollo Cryogenic Oxygen Tank Analysis Meeting. NASA MSC, Houston, Texas, Jan. 1971.
2. Kamat, D. V.; and Abraham, W. H.: Pressure Collapse in Oxygen Storage under Zero-g. J. Spacecraft, 5, 184, 1968.
3. Haron, A. S.: Transient Analysis of Heat Transfer in a Simplified Model of the Apollo Oxygen Tank-Case 320. Memorandum for file. Included in Minutes of Third Apollo Cyrogenic Oxygen Tank Analysis Meeting, NASA MSC, Houston, Texas, Jan. 1971.
4. **Forester**, C. K.; Rule, D. D.; and Patterson, H. W.: Apollo Oxygen Tank Stratification Analysis. Boeing Document No. D2-118357-1, Nov. 1970.
5. Baldwin, B.; and Sheaffer, Y.: Mixing Effectiveness of Vehicle Rotation Reversal in Apollo Oxygen Tanks. Included in Minutes of Third Apollo Cyrogenic Oxygen Tank Analysis Meeting, NASA MSC, Houston, Texas, Jan. 1971.
6. Martin, E. D.; and Baldwin, B. S.: Flow Equations Governing Combined Forced and Natural Convection in a Rotating Tank. Proposed NASA TR.
7. Baldwin, B.; Reinhardt, W. A.; and Sheaffer, Y.: Thermodynamic Interpretation of Incompressible Flow Simulation of Gas Motion in the Apollo Oxygen Tanks. Proposed NASA TR.
8. Reinhardt, W. A.: Calculation of Thermodynamic Properties of Oxygen Near the Critical Point. Proposed NASA TR.
9. Lomax, H.; and Bailey, F. R.: Computational Method for Calculating Convection in a Rotating Square Tank. Proposed NASA TR.
10. Baldwin, B. S.; Reinhardt, W. A.; and Sheaffer, Y.: Results from Numerical Computations Simulating Flows in an Apollo Oxygen Tank. Proposed NASA TR.
11. Hirschfelder, J. O.; Curtiss, C. F.; and Bird, R. B.: Molecular Theory of Gases and Liquids. John Wiley & Sons, New York, 1954, pp. 237, 250-252.
12. Borucki, W. J.: Absorption of Infrared Radiation by High Density Oxygen. To be published in AIAA Journal, May or June 1971.
13. Anon.: Apollo Fuel Cell and Cryogenic Gas Storage System Flight Support Handbook. Prepared by Propulsion and Power Division, NASA MSC, Houston, Texas, Feb. 1970.

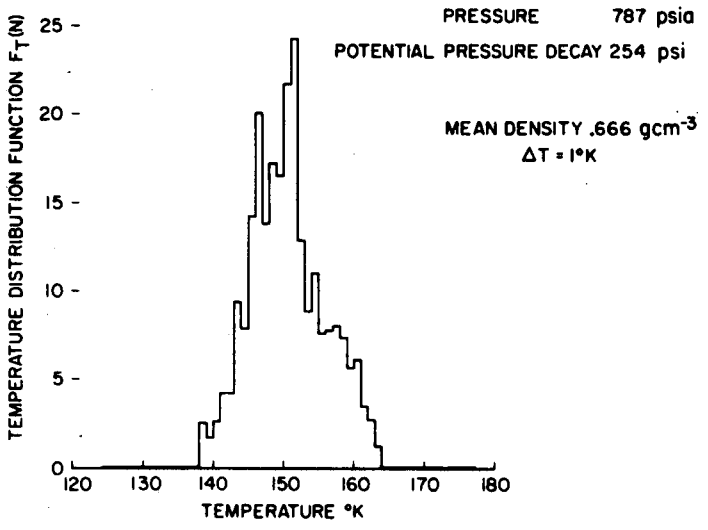

Figure 1. Typical temperature distribution function.

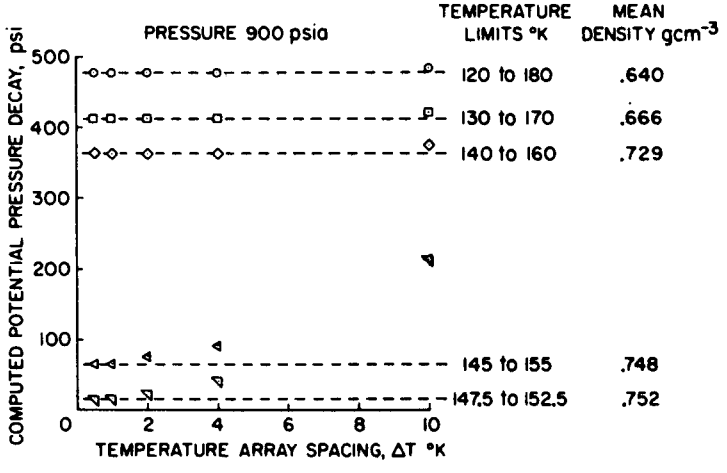

Figure 2. Effect of temperature array spacing on computed potential pressure decay.

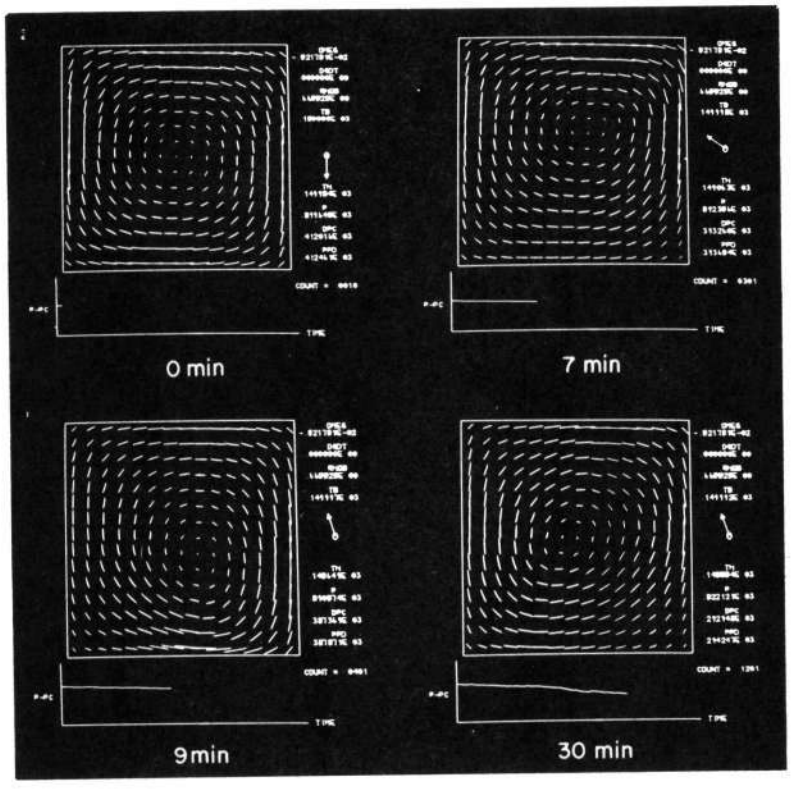

Figure 3. Velocity vectors after rotation reversal.

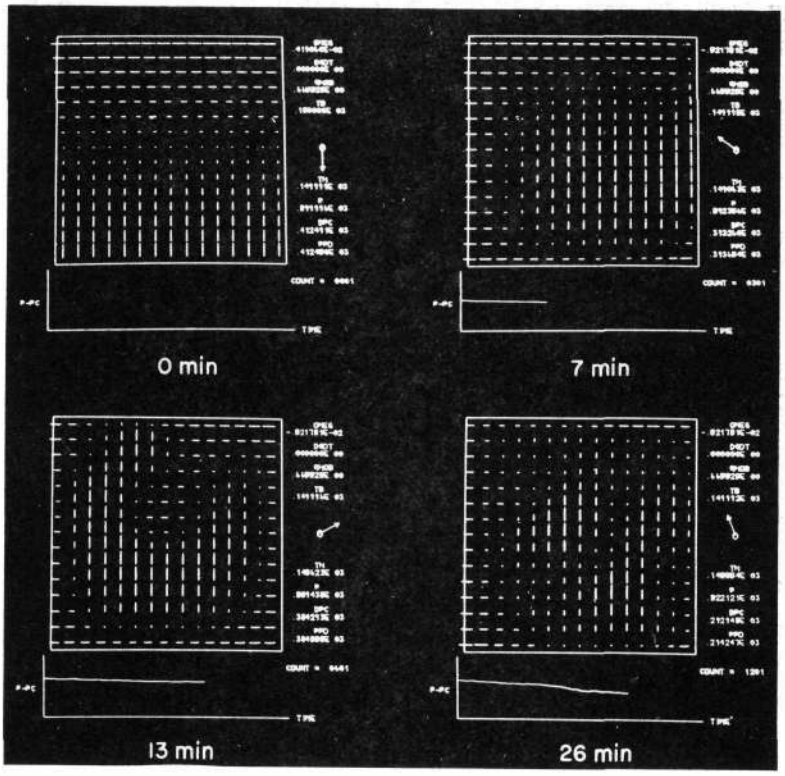

Figure 4. Temperature distributions after rotation reversal.

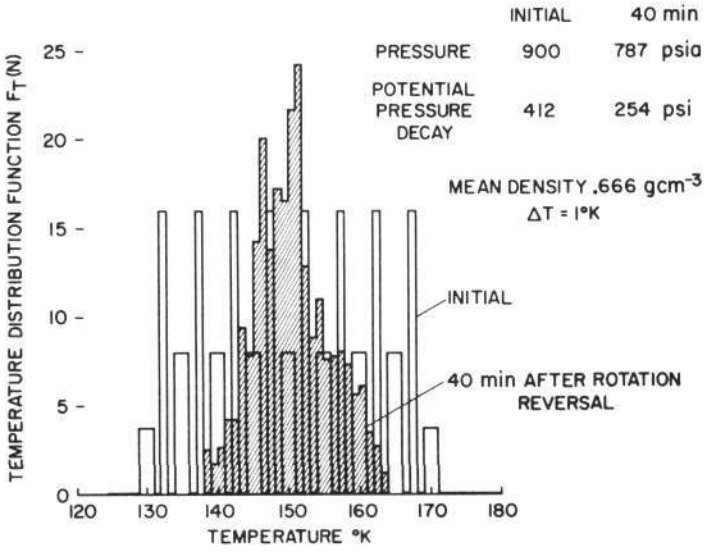

Figure 5. Temperature distribution functions.

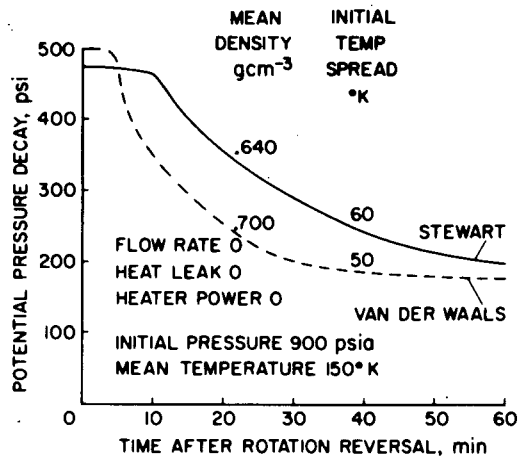

Figure 6. Comparison of potential pressure decay for van der Waals and exact thermodynamics.

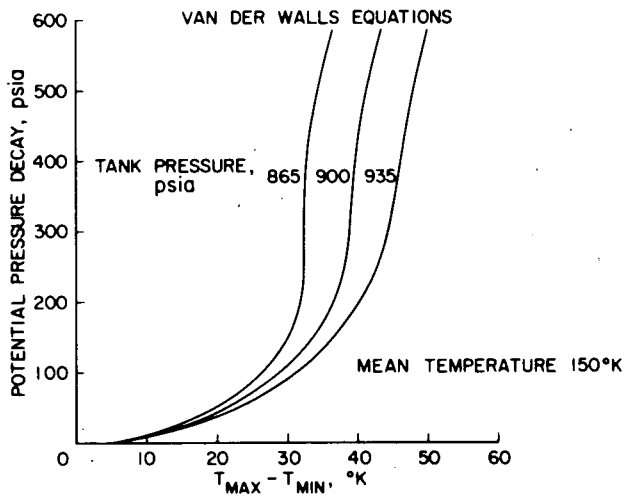

Figure 7. Potential pressure decay for linear temperature variations; van der Waals equations.

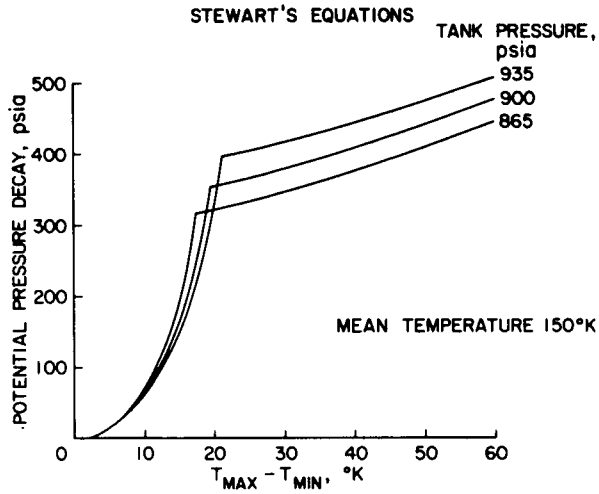

Figure 8. Potential pressure decay for linear temperature variations; Stewart's equations.

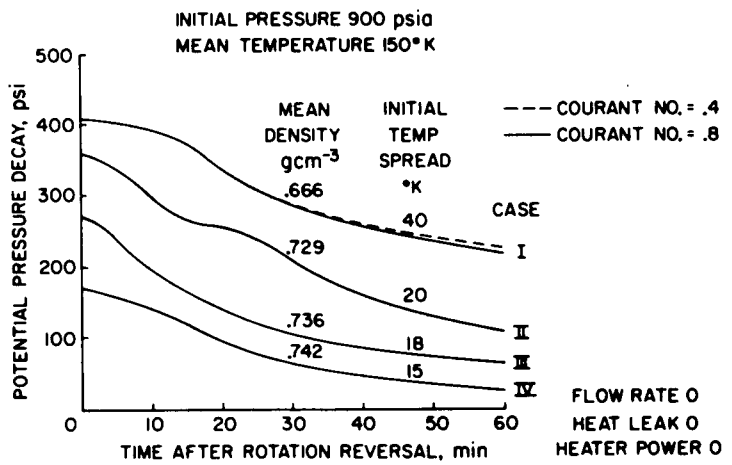

Figure 9. Potential pressure decay after rotation reversal.

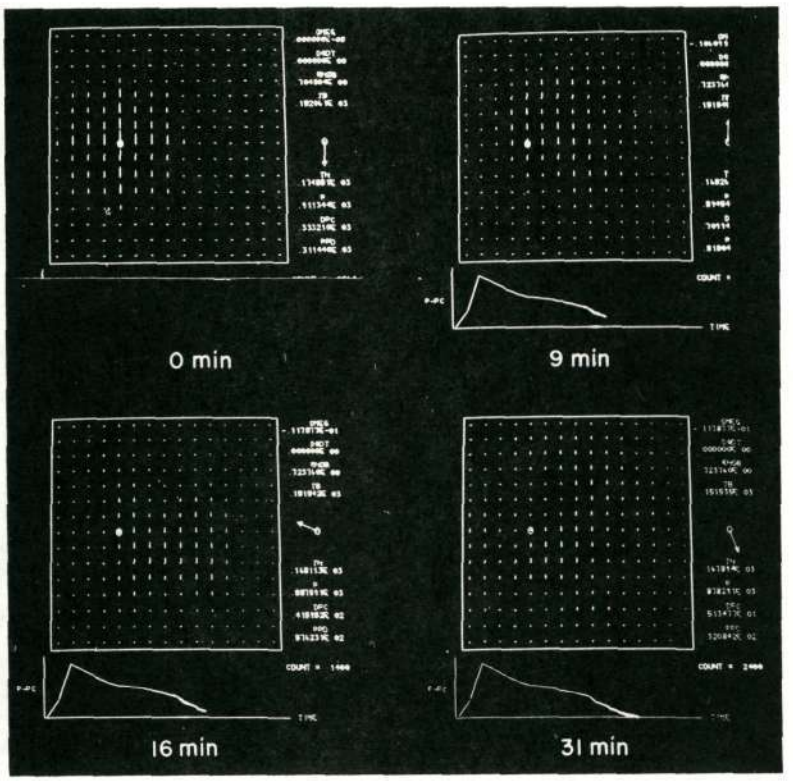

Figure 10. Temperature distributions after spin-up.

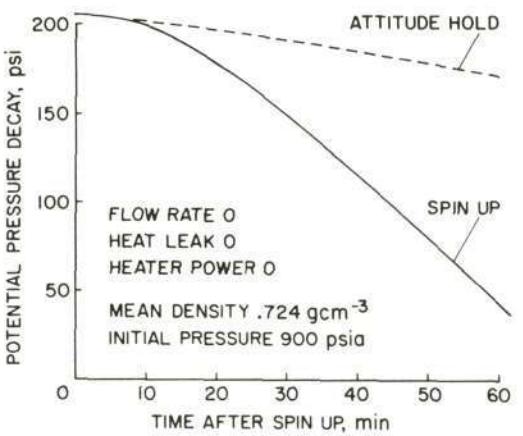

Figure 11. Reduction in potential pressure decay due to spin-up.

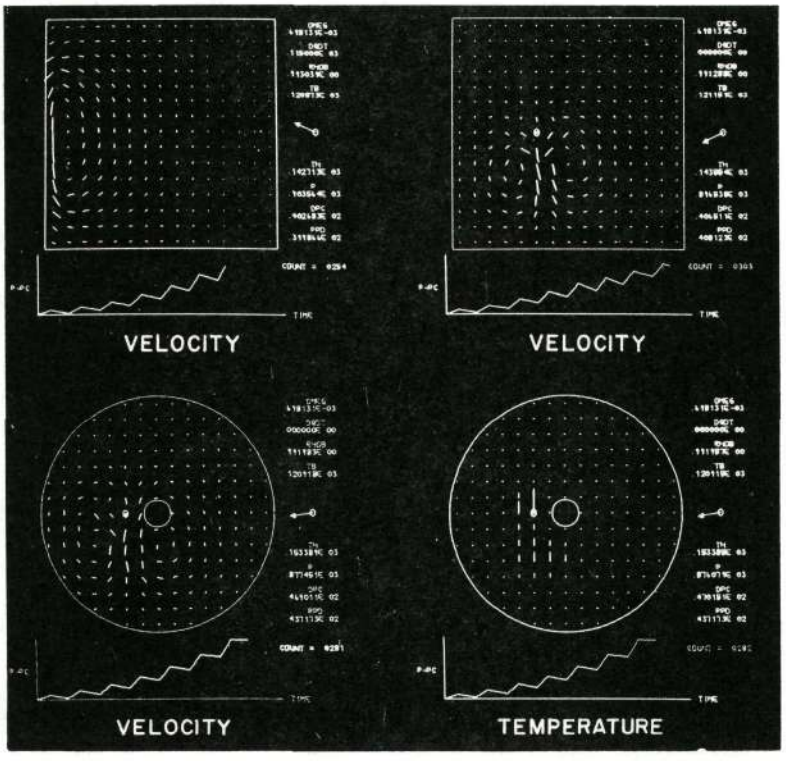

Figure 12. Velocity and temperature distributions resulting from heater operation.

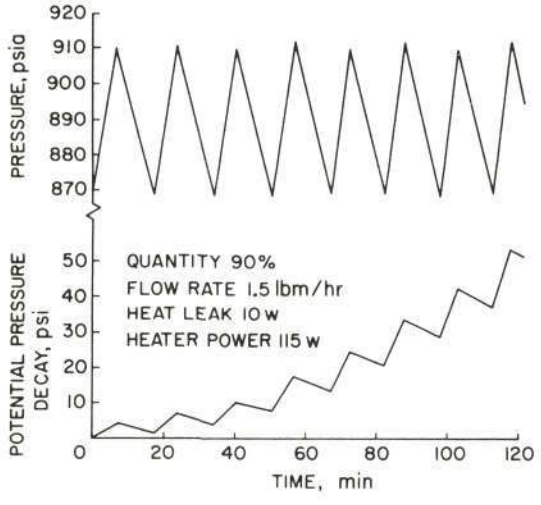

Figure 13. Pressure cycles for square tank with wall heater.

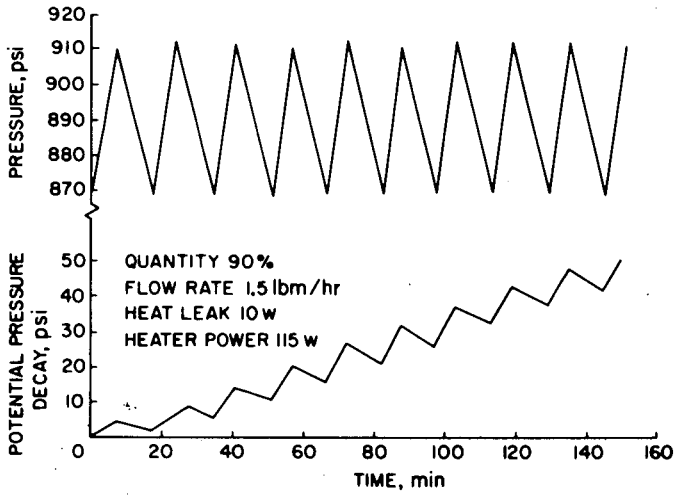

Figure 14. Pressure cycles for square tank with off-center heater.

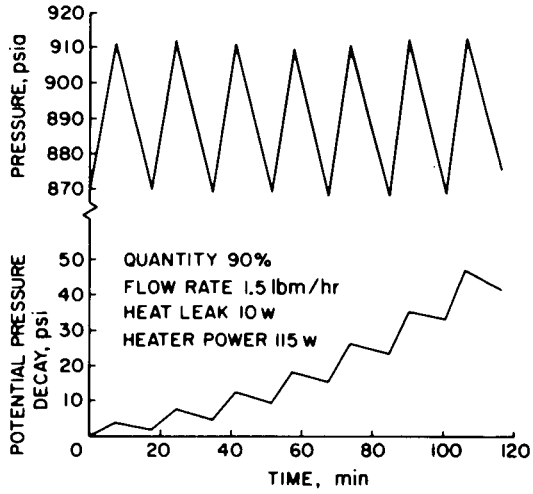

Figure 15. Pressure cycles for circular cylindrical tank.

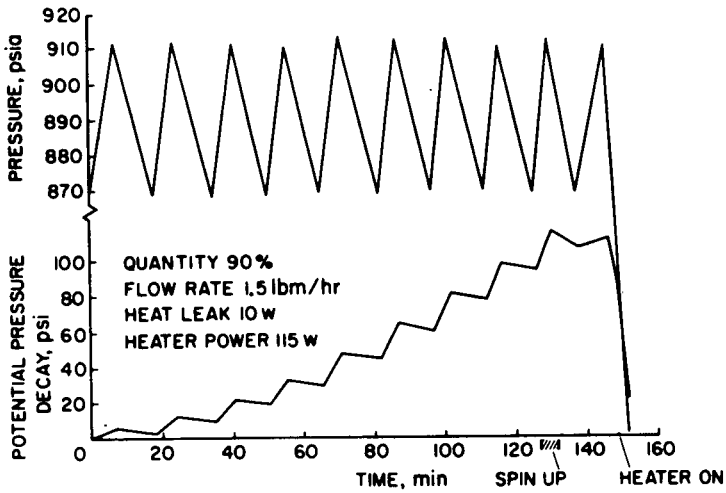

Figure 16. Effect of spin-up on pressure cycle (circular cylindrical tank).